

# Inkjet-Printed p-NiO/n-ZnO Heterojunction Diodes for Photodetection Applications

Sergio González, Giovanni Vescio,\* Juan Luis Friero, Alina Hauser, Flavio Linardi, Julian López-Vidrier, Marek Oszajca,\* Sergi Hernández, Albert Cirera, and Blas Garrido

Transparent Conducting Oxides (TCOs) are an enticing family of optoelectronic materials which have been proven to increase efficiency when incorporated into perovskite light emitting diode (PE-LED) and organic OLED architectures as transport layers. Solution-processed metal oxide inks have already been demonstrated, although there is still a need for high-quality inkjet-printable metal oxide inks with a thermal post-process below 200 °C. The set of inks in this work are adapted from low-boiling point colloidal suspensions of metal oxide nanoparticles synthesized via flame spray pyrolysis. High quality, pinhole- and wrinkle-free inkjet-printed layers are obtained at low temperatures through vacuum oven post process, as proven by scanning electron microscopy. The crystallinity of the layers is confirmed by X-ray diffraction, showing the expected hexagonal and cubic structures respectively for ZnO and NiO. The thin film layers reach over 70% (ZnO) and 90% (NiO) transparency in the visible spectrum. Their implementation in the inkjet-printed p–n diode shows excellent *I*–*V* rectifying behavior with an ON/OFF ratio of two orders of magnitude at ±3 V and a forward threshold voltage of 2 V. Furthermore, the device exhibits an increase in photocurrent around four orders of magnitude when illuminated under a 1-sun solar simulator.

of large-area and thin film devices. Hydrogenated amorphous silicon (a-Si:H) proved to be key for solar cells and for thin-film transistors (TFTs) used in display electronics. However, problems like low carrier mobility (0.5–1.0 cm<sup>2</sup> V<sup>-1</sup> s<sup>-1</sup>), optical opacity and lack of mechanical flexibility hampering its applicability for future devices.<sup>[1,2]</sup> Organic semiconductor compounds have thrived in OLED applications. These materials have good hole and electron transport properties, yet they exhibit sensibly low intermolecular forces, imposing heavy restrictions on post-processing treatments.<sup>[2]</sup> Furthermore, organic compounds tend to have multiple optical transitions in the visible range, limiting transparency and purity of the emission.<sup>[2]</sup> In addition, they can be considerably costly<sup>[3]</sup> and may rapidly degrade with time.<sup>[4]</sup>

To circumvent these constraints, researchers have dedicated efforts to promising alternatives. One such option lies in transparent-conducting wide band-

gap metal oxides such as ZnO, NiO, SnO<sub>2</sub>, TiO<sub>2</sub> and many others. Compared to their more classical counterparts, TCOs show carrier mobilities competitive even with those of single-crystalline Si,<sup>[1,5–8]</sup> and they are usually abundant. Additionally, they are durable and show high mechanical stress tolerance, which makes them suitable for flexible optoelectronics.<sup>[2]</sup> Last but not least, high-quality TCO thin layers can be obtained through simple solution processing techniques.<sup>[2]</sup>

Semiconducting electrical properties of metal oxides have been reported since the late 50s.<sup>[9]</sup> Single crystal ZnO and other II-VI materials have been used for many years in optoelectronics.<sup>[5,10]</sup> More recently, the research of T. Kamiya and H. Hosono in 2004 in large-area metal oxide semiconductors, focused on an Indium Gallium Zinc Oxide (IGZO) applied to transparent TFT,<sup>[5,11]</sup> became the standard in demanding display applications.

Conventional device manufacturing techniques, like sputtering, thermal evaporation, or chemical vapor deposition (CVD), are the most commonly employed ones to deposit these materials. However, these techniques typically require costly high-vacuum and high-temperature processes in addition to the masking or photolithography procedures necessary to define the desired device geometry, thus increasing manufacturing overhead and limiting the maximum throughput.<sup>[12,13]</sup>


## 1. Introduction

The expanding market of optoelectronic devices is ever-growing, from light-emitting diodes (LEDs) and displays to photovoltaic devices and photodetectors. In the field of optoelectronics, different classes of materials have been pivotal to the development

S. González, G. Vescio, J. L. Friero, J. López-Vidrier, S. Hernández, A. Cirera, B. Garrido  
 MIND-IN2UB

Department of Electronics and Biomedical Engineering  
 Universitat de Barcelona  
 Martí i Franquès 1, Barcelona 08028, Spain  
 E-mail: gvescio@ub.edu

A. Hauser, F. Linardi, M. Oszajca  
 Avantama AG  
 Laubisruetistrasse 50, Staefa 8712, Switzerland  
 E-mail: marek.oszajca@avantama.com

 The ORCID identification number(s) for the author(s) of this article can be found under <https://doi.org/10.1002/admi.202300035>.

© 2023 The Authors. Advanced Materials Interfaces published by Wiley-VCH GmbH. This is an open access article under the terms of the Creative Commons Attribution License, which permits use, distribution and reproduction in any medium, provided the original work is properly cited.

DOI: 10.1002/admi.202300035

An alternative to conventional device manufacturing technologies are the solution-based fabrication approaches, which are receiving exceptionally great attention. Nowadays, technologies such as screen printing and inkjet IJP, which have been used extensively in the graphics arts industry, are being used to deposit functional materials. Screen printing requires the use of masks and direct contact with the substrate, both of which are added challenges for fast prototyping, and it is generally indicated when thicknesses over 10  $\mu\text{m}$  are required. Complementary to screen printing, IJP is maskless and contactless, and it provides a method to produce low-cost, large-area, lightweight, and foldable devices. Several inks of a diversity of materials for optoelectronic applications are currently available commercially. Besides, the huge demand for new flexible printed electronic devices pushed the formulation of functional inks in the form of precursor inks, nanoparticle colloidal suspensions, nanocrystal solutions, or organo-metallic compounds.<sup>[14,15]</sup>

As opposed to using a mask, IJP allows the direct deposition of inks in a specified pattern with high precision. In particular, the model series Dimatix DMP-2850, the most used in the research area for validating the processing scalability, reaches  $\pm 5 \mu\text{m}$  mechanical repeatability in drop placement, allowing an ordered printed drop density of 1000 drop-per-inch (DPI), and drop volume control from 1 to 10 pL, easily covering an A4 area in few minutes. These characteristics make IJP ideal for fast prototyping while having potential for scalability,<sup>[16]</sup> a very attractive combination of properties for those aiming towards high-volume commercialization.<sup>[17–19]</sup> Thus, mass-scale, relatively simple and cost-effective production of electronic devices is made possible by leveraging the maturity of IJP as a material deposition technique. One major challenge of IJP is the fabrication of uniform and pinhole-free layers over a large area. Factors influenced by using various materials and the nature of solutions increase printing complexity.<sup>[20,21]</sup> This can be addressed by appropriate ink formulation and substrate preparation.

Advances in ink formulation, control of rheology and ink stability have led to the achievement of fully-inkjet printed devices in a variety of fields, including OLEDs, solar cells, and graphene transistors.<sup>[21–24]</sup> Despite the relevant progress in device fabrication, until recently, the application of metal oxide inks to IJP has remained challenging, due to the relatively limited availability, and the fact that most solutions required relatively high temperature post-treatments (400  $^{\circ}\text{C}$ ).<sup>[25]</sup> The high temperature requirement places constraints not only on the substrate, barring the use of possible flexible materials, but also on the previous layers. This is especially true for device architectures combining organic and inorganic compounds.<sup>[13,26]</sup>

As a wide direct bandgap semiconductor (with a bandgap energy of  $E_g = 3.37 \text{ eV}$ ), ZnO is one of the most promising and versatile options for transparent ultraviolet (UV) optoelectronics.<sup>[6,27–30]</sup> Although it is well known to have lost the race to the blue LED in favor of high-quality and crystalline epitaxial GaN, ZnO is still the material of choice for solution-based large-area polycrystalline optoelectronics.<sup>[31,32]</sup> Consistently, many of the ZnO applications might overlap with those of GaN, including UV/blue LEDs thanks to its high exciton binding energy of 60 mV,<sup>[2,27]</sup> abundant availability and lower fabrication cost.<sup>[2,33,34]</sup>

Although ZnO homojunction LEDs have been achieved, compared to an *n*-type ZnO layer, obtaining a stable and reproducible *p*-type ZnO layer is rather problematic.<sup>[27,28]</sup> Thus, other *p*-type alternatives should be explored to achieve *p*–*n* heterojunctions with ZnO. In particular, NiO is a *p*-type direct bandgap semiconductor ( $E_g = 3.7 \text{ eV}$ ) which is also an inexpensive, abundant, environmentally friendly option well-known as a hole transport layer due to its intrinsic *p*-type character.<sup>[35–37]</sup> It has been shown to be compatible with ZnO for fabricating optoelectronic devices by other methods, like CVD and sputtering.<sup>[38–45]</sup>

In this paper we present results relative to the IJP fabrication and characterization of an inorganic conductive transparent NiO/ZnO heterojunction photodetector, obtained with thermal processes below 200  $^{\circ}\text{C}$ .

The characterization of *p*-type NiO and *n*-type ZnO individual layers is presented first, followed by a thorough characterization to determine morphology, composition, and crystallinity through SEM and XRD. Subsequently, the fabrication and device characterization of a heterojunction diode with a device structure of Au/NiO/ZnO/C is introduced. Au has a work function that, corresponded with NiO bands, results in an ohmic contact,<sup>[46]</sup> and, as a noble metal, it ensures a good electrical interface. Finally, the dark intensity–voltage (*I*–*V*) characteristics of the devices are presented and compared to their counterpart under illumination.

## 2. Results and Discussion on Inkjet Printed NiO/ZnO Layers

### 2.1. Morphology and Crystalline Structure

The expected device architecture, the band structure and a top-view photograph of the devices after deposition of the layers, are represented in **Figure 1**.

The NiO and ZnO layers were cured in a vacuum oven for improved layer quality. Vacuum curing is crucial for obtaining high-quality layers, as it ensures solvent evaporation at relatively low temperatures and avoids exposure to atmospheric contaminants such as moisture during oven processing.<sup>[47,48]</sup> **Figure 2** shows a comparison in quality of both NiO and ZnO layers with and without employing vacuum, both cured at 200  $^{\circ}\text{C}$ . In NiO layers cured in atmospheric conditions, the texture of the layer cannot be clearly discerned in SEM, a common occurrence in layers with incomplete drying (Figure 2a).<sup>[49]</sup> Instead, the layers dried in vacuum show clear contrast of the granules that form it, an indication of a more thorough drying of the solvents.

Indeed, improvements in layer quality can be observed in Figure 2b,d. The printed thin film presents, when drying with no vacuum, the appearance of nonuniformities in the form of dark regions in the otherwise homogeneous thin layer, which might indicate marked localized bubbling of the solvent as it evaporates. The precise origin of this phenomenon promotes clear undesired pinholes into the layer. However, upon switching to drying the inkjet-printed layers under vacuum process a pinhole-free layer is observed, again pointing to vacuum curing as the most controlled and feasible thermal process.

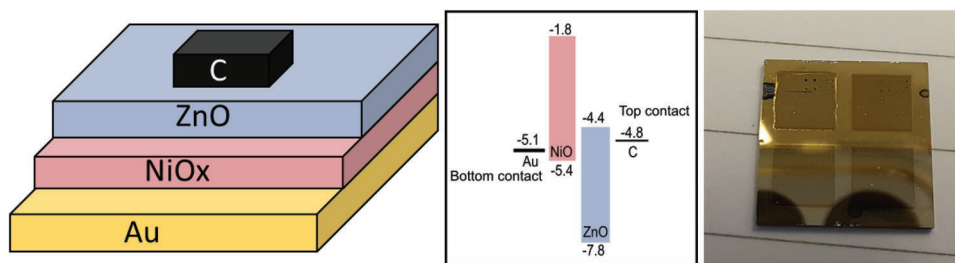


**Figure 1.** a) Cross-section diagram of p–n diode, b) band diagram of structure Au/NiO/ZnO/C at equilibrium and c) top-view photograph of the device deposited on the Si/Au substrate.

**Figure 3** shows details of the field emission scanning electron microscopy (FE-SEM) images of single layers of NiO and ZnO obtained through inkjet printing on Si/SiO<sub>2</sub> substrates and cured at 200 °C for 1 h in vacuum. In both cases, homogeneous, compact, polycrystalline, and continuous layers can be clearly observed. As expected, some surface granularity at this scale is observed, with an approximate grain size of 35–50 nm for ZnO and 28–35 nm for NiO, as measured from the micrographs. These grain sizes are larger than the nanoparticle size in ink solution, pointing to successful annealing. Additionally, the layers do not show pinholes or cracks, indicating that the printed layers are of high quality and suitable for charge transport applications.

**Figure 4** shows the XRD patterns from the inkjet-printed layers of ZnO and NiO, respectively. ZnO shows multiple diffraction peaks (Figure 4a), which can be identified as its wurtzite crystal structure (hexagonal system). ZnO can exist in three different crystalline structures: rock-salt, zinc blende and wurtzite. Of these, only wurtzite is thermodynamically stable at normal atmospheric conditions,<sup>[50,51]</sup> thus confirming that

we have achieved the expected crystalline phase of ZnO. Of the other phases, rock-salt would require synthesis at high pressure, and zinc-blende a synthesis on a cubic substrate.<sup>[52]</sup>

In the case of NiO, we observe three peaks corresponding to NiO in its cubic phase (Figure 4b), which is the only crystalline system commonly reported for this material, in a rock-salt crystalline structure. The average crystallite size can be estimated from the full-width at half-maximum (FWHM) of these peaks using the Debye–Scherrer equation (Equation 1):

$$\tau = \frac{K\lambda}{\beta \cos(\theta)} \quad (1)$$

where  $\lambda = 0.15406$  nm is the wavelength of X-ray radiation,  $B$  is the FWHM and  $\theta$  is the diffraction angle. The values obtained for ZnO and NiO layers are 13 and 9 nm, respectively. These values are in accordance with and support the values of nanoparticle size in suspension reported for these inks, respectively 12 and 7 nm. The results from FESEM combined with the XRD data confirm that the nanoparticles did indeed sinter, but not

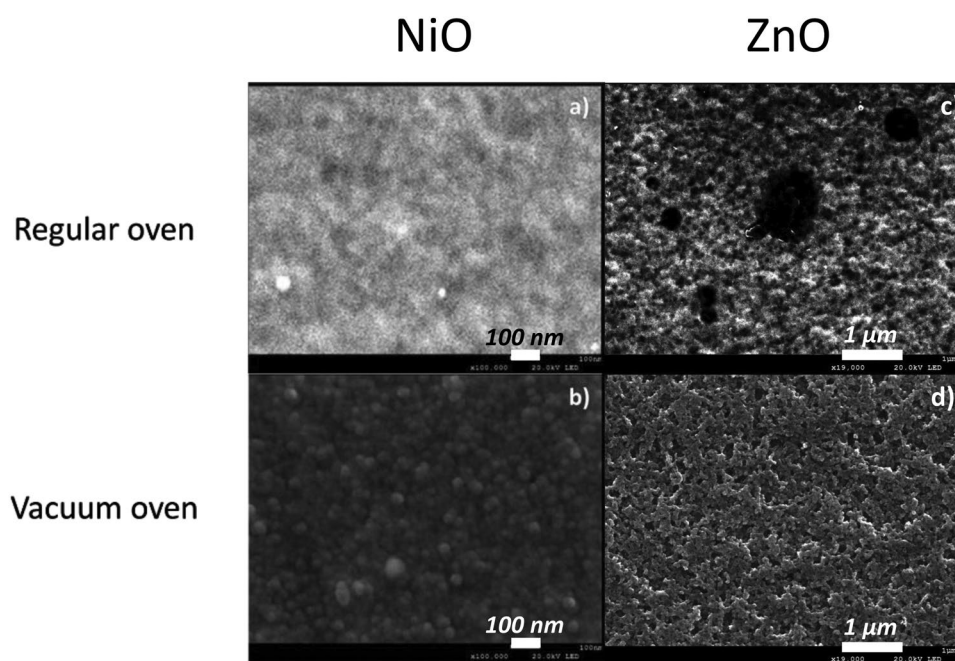


**Figure 2.** SEM images of layers of NiO and ZnO cured in a regular oven and vacuum oven, showing an improvement in layer quality when cured in the latter.

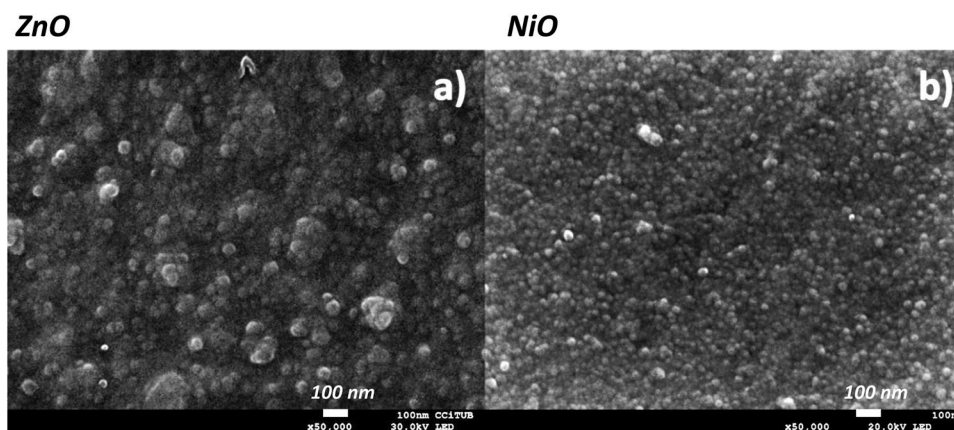


**Figure 3.** Details of the top view micrographs of layers of a) ZnO and b) NiO obtained by inkjet printing and cured in a vacuum oven at 200 °C for 1 h.

recrystallize in a different phase, like obtained in other consolidated techniques such as atomic layer deposition or CVD.<sup>[53,54]</sup>

## 2.2. Optical Properties

To study the optical properties of our device, both NiO and ZnO layers have been printed on fused silica, which has better transparency in the UV than regular glass (see **Figure 5a,b**), thus allowing to perform transmittance and reflectance measurements in the visible and near-UV spectrum, in order to determine their absorbance and band-gap energy value.

In parallel, we also inkjet-printed layers of NiO and ZnO on flexible substrates, demonstrating that high-quality layers can be obtained in both cases. The related images in **Figure 5c–e** show macro photographs of 1 × 1 cm<sup>2</sup> areas of both NiO and ZnO inkjet-printed thin films on to a polyethylene terephthalate (PET)

substrate. The layers appear homogeneous across the relatively large area. The color seen in the layers comes from reflected light, and thus it gives an idea of the layer thickness through interference within the inkjet-printed thin films. The ZnO layer shows an increase in thickness in the edges of the printed area, a well-known phenomenon in printed layers known as coffee-ring.<sup>[55]</sup> This, however, is clearly localized in the edge area, whereas the rest of the printed square remains homogeneous.

As TCOs, NiO and ZnO should provide high transparency in addition to electrical conductivity. Nevertheless, the presence of defects or free carriers, as well as the reflectance due to the high contrast in refractive indices in air, imposes a limit on the maximum transparency that can be achieved. The reflectivity due to the high refractive index ( $n$ ) contrast can be estimated using the formula (Equation 2):

$$R_{n_2-n_1} = \left( \frac{n_2 - n_1}{n_2 + n_1} \right)^2 \quad (2)$$

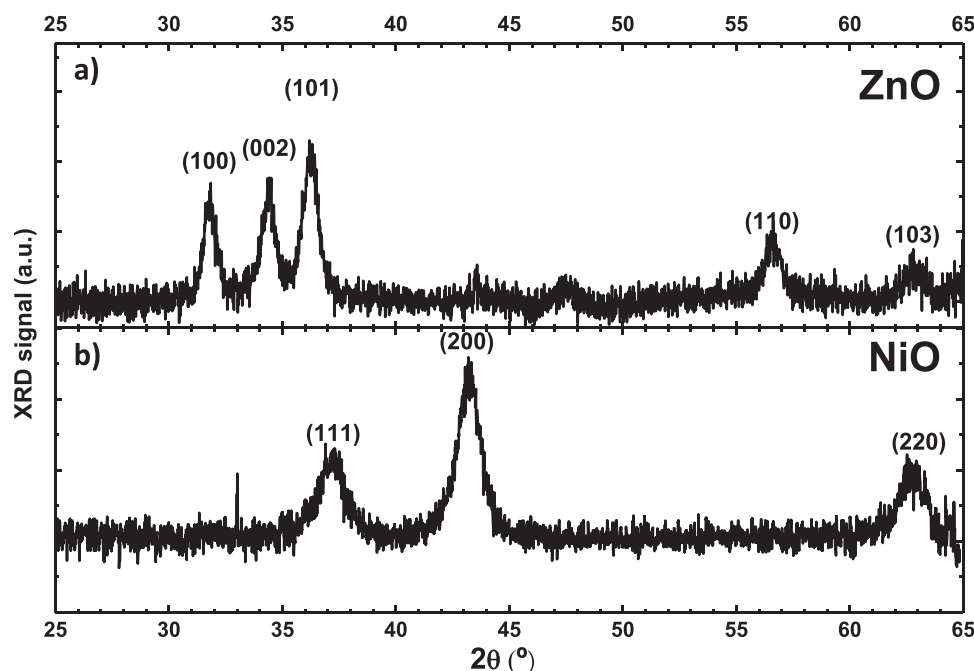


**Figure 4.** XRD patterns of a) ZnO and b) NiO inkjet-printed layers.

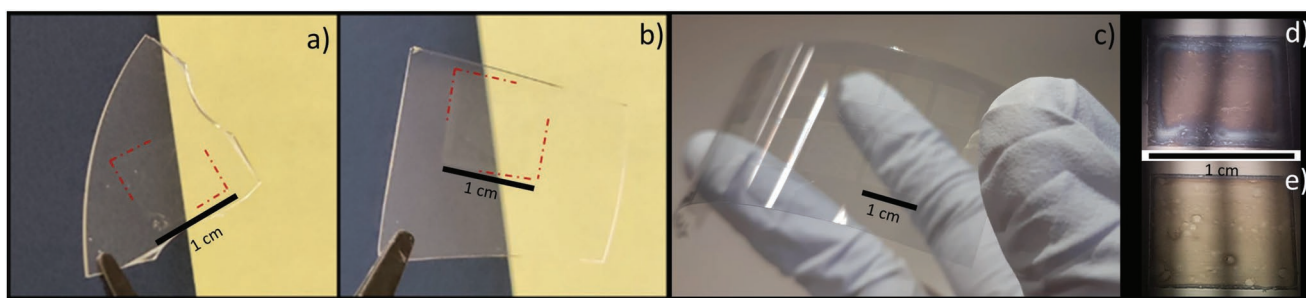


**Figure 5.** Close-up images of layers of a) ZnO and b) NiO deposited on fused silica substrates. Red lines outline the printed areas. c) ZnO and NiO layers printed on flexible substrates, shown in detail in d) ZnO and e) NiO.

From this, it follows that the maximum value of transmittance is (Equation 3):

$$T_{\max} = 1 - R_{n2-n1} \quad (3)$$

Assuming  $n_{\text{ZnO}}$  (at  $\lambda = 500 \text{ nm}$ ) = 2.018<sup>[56]</sup> and  $n_{\text{NiO}}$  (at  $\lambda = 500 \text{ nm}$ ) = 2.18,<sup>[57]</sup> the corresponding  $T_{\max}$  for ZnO and NiO is 88.6% and 86.2%, respectively.

**Figure 6** displays the results of the optical characterization of inkjet-printed NiO and ZnO layers, compared with the transmittance spectrum of the fused silica substrate. Both materials present high transmittance in the visible spectrum, above 90% for NiO (Figure 6a) and 70% for ZnO (Figure 6b), respectively. For wavelengths close to, but higher than, the band gap of ZnO, there is a decrease in its transmittance, as evidenced for wavelengths shorter than 375 nm (3.30 eV). Furthermore, the measured transmittance of ZnO and NiO is very close to the estimated values of  $T_{\max}$  due to the high contrast of refractive indices with the air (Equation 3).

Following, **Table 1** shows a comparison of transmittance and coefficient of absorbance in the range of 400–600 nm light of similar NiO and ZnO thin films found in the literature. The coefficient of absorbance is used because it eliminates the dependence on layer thickness when comparing the optical characteristics of layers with different thicknesses. Without absorbance information, it is difficult to determine the coefficient of absorbance of thin films with accuracy. The coefficient of absorbance was nevertheless estimated using the exponential law of absorption (Equation 4) assuming no reflectance as

most references only include transmittance but not absorbance measurements.

$$\alpha = -\frac{1}{t} \ln(T) \quad (4)$$

A comparison between the absorption coefficients of our layers and of similar layers found in the literature, produced with more consolidated techniques, is shown in Table 1. As can be observed, the obtained absorption coefficients for our inkjet-printed layers are comparable than for similar layers in the literature.

Using the reflectance and transmittance measurements, the absorbance can be straightforward evaluated ( $A = 1 - R - T$ ) and, by using a Tauc plot for direct band-gap materials, the band-gap energy of the inkjet-printed layers can be determined according to the relation:

$$(\alpha \cdot h \cdot \nu)^2 \propto (h \cdot \nu - E_g) \quad (5)$$

where  $h\nu$  is the photon energy, and  $\alpha$  is the absorption coefficient that can be determined from the absorbance ( $A = e^{-\alpha \cdot d}$ , being  $d$  the thickness of the layers). A plot of these quantities is provided in Figure 6c. A linear regression in this graph provides an estimation of the optical bandgap of the inkjet-printed ZnO layer at  $\approx 3.28 \text{ eV}$  (378 nm). This is in close agreement with literature, demonstrating that the optical properties of the inkjet-printed ZnO thin films are obtained as expected. In the case of NiO, its bandgap falls outside the measurement window

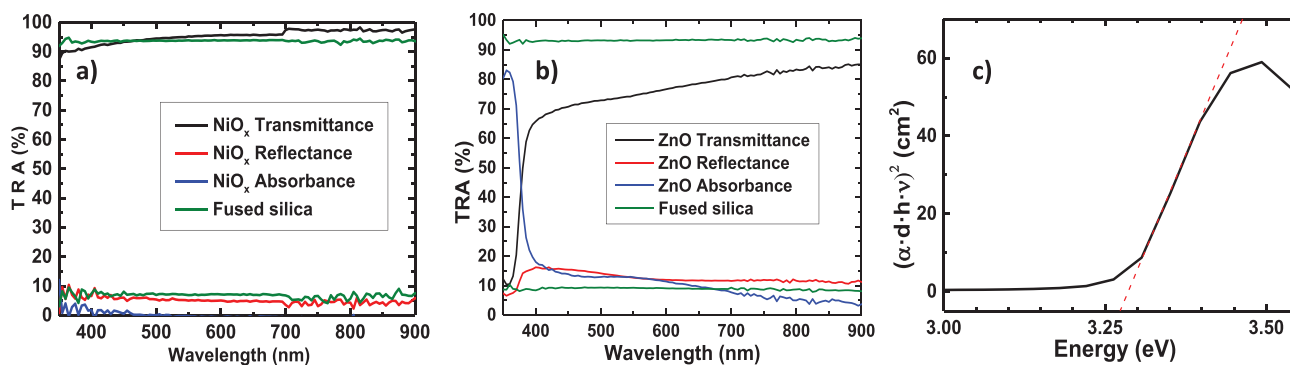


**Figure 6.** Optical measurements of NiO and ZnO. a) Transmittance, reflectance, and absorbance of b) NiO and of ZnO. The transmittance of the fused silica substrate is given for the sake of comparison. c) Tauc plot of ZnO and corresponding fit to determine its optical band gap energy.

**Table 1.** Comparison of absorption coefficients of similar layers of NiO and ZnO found in the literature.

Ref.	Material	Method	Thickness [nm]	Transmittance range [%] [400–600 nm]		Coeff. Abs Range [400–600 nm] [1/ $\mu\text{m}$ ]	
this work	NiO	Inkjet	200	90	95	0.53	0.26
[58]	NiO	Spin coating	40	87	95	1.94	0.40
[59]	NiO	Epitaxy	50	97	98	0.61	0.40
[60]	NiO	Chemical bath deposition	120	88	88	1.07	1.07
[61]	NiO	Spin coating	150	88	92	0.85	0.56
this work	ZnO	Inkjet	200	65	80	2.15	1.12
[62]	ZnO	Spin coating	100	67	90	4.00	1.05
[63]	ZnO	Sol-gel	200	85	90	0.81	0.53
[64]	ZnO	Ultrasonic spray pyrolysis	200	80	92	1.12	0.42
[65]	ZnO	Spin coating	150	88	92	0.85	0.56

of our system ( $\lambda > 350$  nm), around  $\approx 3.7$  eV (335 nm), and thus is not obtainable via Tauc plot representation.<sup>[66]</sup>

### 2.3. Electrical Characterization of the PN Junction

In order to study the electrical properties of the inkjet-printed Au/NiO/ZnO/C heterojunction, the  $I$ - $V$  characteristics of a device of area  $0.03$  mm<sup>2</sup> (Figure 7a) was measured in dark. The active device area is determined by the top carbon contact, with a radius of  $100$   $\mu\text{m}$ . Complementary, Figure 7b represents the  $I$ - $V$  characteristics of the device under AM 1.5 illumination. The heterojunction displays excellent current rectification behavior, with a large current ratio between forward and reverse polarizations of two order of magnitude at  $\pm 3$  V, and a threshold voltage of about  $2.2$  V. The following Table 2 compares the results in this work with the rectification properties of similar devices in the literature fabricated by more established processes.

The photoresponse properties of the inkjet-printed Au/NiO/ZnO/C device were also studied by measuring its  $I$ - $V$  characteristics under illumination from a solar simulator. Figure 7b compares the  $I$ - $V$  characteristics of the

heterojunction in dark and under illumination (in semi-log scale, taking the current intensity in absolute value). An outstanding ratio of 4 orders of magnitude in current is observed for the inverse polarization under an AM1.5 Global solar simulator.

### 3. Conclusion

We present the first results of a NiO/ZnO heterojunction thin film photodetector fabricated in ambient conditions through inkjet printing technology. High-quality individual layers of NiO and ZnO have been obtained, being compact, with no surface defects, and with high transparency (70–90%) in the visible range. The complete device shows clear rectifying behavior in the dark, and a marked wide band photoresponse when exposed to AM1.5 Global solar simulator light, realized as an exceptional four order of magnitude ratio in current at inverse polarization. These are encouraging results, demonstrating that the fabrication of optoelectronic devices, based on abundant and environmental-friendly inorganic transition metal oxide semiconductors, using the maskless, scalable inkjet printing technology is feasible.

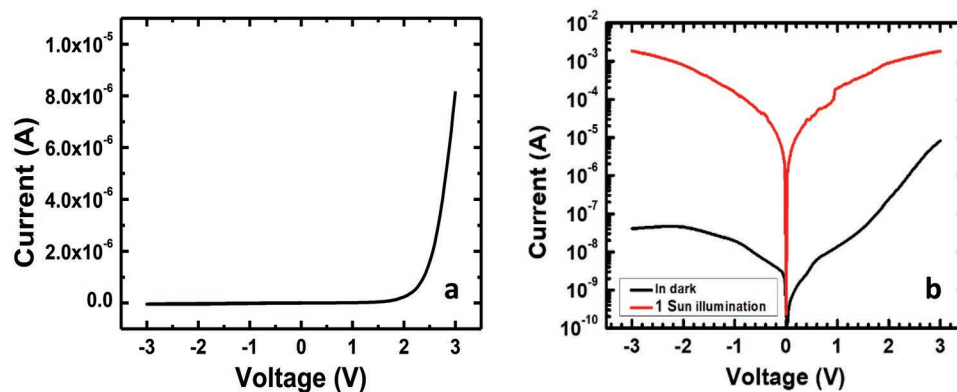


**Figure 7.** a) Linear representation of the  $I$ - $V$  characteristics of the heterojunction in dark. b) Semilog graph of dark and illuminated  $I$ - $V$  curves of the Au/ NiO / ZnO/ C heterojunction. In both graphs, current is presented in absolute value.

**Table 2.** Comparison of the rectification properties of similar devices in the literature.

Ref.	Structure	Device	Deposition method	$\log_{10}[I_{\text{f}}/I_{\text{r}}]$	measured @voltage [V]
this work	Au/NiO/ZnO/C	UV photodetector	Inkjet printing	0.8	2
[67]	ITO/NiOx/ZnO/Al	UV photodetector	Spin coating	2.46	1
[68]	ITO/NiOx/ZnO/Al	UV photodetector	Spin coating	2.05	5
[69]	Au/NiOx/ZnO/Au	UV photodetector	RF magnetron sputtering	3.81	2
[70]	ITO/ZnO/NiO/Ni	UV photodetector	Sputtering (ZnO) + ion beam (NiOx)	3.60	2
[71]	ITO/NiO/ZnO/Au	UV photodetector	PLD(ZnO) + solid phase epitaxy (NiO)	2.36	2
[72]	ITO/In <sub>2</sub> O <sub>3</sub> /NiO/PEDOT:PSS	Diode	Inkjet printing	1.04	2

## 4. Experimental Section

**Preparation of the Inks for Printing ZnO and NiO:** For the deposition of the ZnO and NiO layers, metal oxide nanoparticle inks based on hexanol provided by Avantama AG had been used. The dry ZnO and NiO nano powder was prepared by flame spray synthesis using a precursor solution of zinc and nickel acetate in 2-ethylhexanoic acid, respectively for ZnO and NiO; the solution was diluted with 30 wt% xylene. The precursors then were fed (7 mL min<sup>-1</sup>) to a spray nozzle, dispersed by oxygen (9 L min<sup>-1</sup>) and ignited by a premixed methane-oxygen flame (CH<sub>4</sub> : 1.2 L min<sup>-1</sup> and O<sub>2</sub> : 2.2 L min<sup>-1</sup>). The off-gas was filtered through a steel mesh filter (20 μm mesh size) by a vacuum pump at about 20 m<sup>3</sup> h<sup>-1</sup>. The obtained ZnO and NiO nano powders were collected from the filter mesh. A stable suspension was prepared by dispersing 2.5 wt% ZnO and NiO nano powder in hexanol using an undisclosed dispersant (proprietary information of Avantama AG). The ZnO ink had a solid content of 2.5 wt%, particles of 12 nm size, and a viscosity of 5 cP. The NiO ink had a solid content of 2.5 wt%, particles of 7 nm size, and a viscosity of 5 cP. C contacts were deposited from a commercial carbon conductive paste from Bare Conductive.

**Device Fabrication:** Single layers of either ZnO or NiO had been deposited on different substrates: Si/SiO<sub>2</sub> was used for morphological measurements (SEM). Fused silica was used for optical measurements. Glass slides were used for Van der Pauw measurements. Au-covered Si substrates were used for the heterojunction. The substrates were cleaned with a three-step process of Hellmanex detergent, acetone, and isopropanol. They were sonicated at 40 °C for 5 min at every step and afterward rinsed with ultrapure water at boiling temperature, and blown with N<sub>2</sub> at the last step. Once the substrates were cleaned, ZnO or NiO inks were printed on top using a Dimatix 2850, at a drop spacing of 30 μm, which ensured proper wetting of the surface. After printing, the metal oxide films underwent a curing process at 200 °C for 1 h in a vacuum oven. Adequate curing temperatures had been determined in accordance with thermogravimetry measurements. The heterojunction fabrication process was as follows: first, NiO was printed at 850 DPI obtaining a final thickness of ≈500 nm and then dried at a vacuum oven at 200 °C for 1 h, followed by IJP ZnO at 850 DPI with a final thickness of ≈500 nm, and again drying it inside the vacuum oven at 200 °C. Finally, the carbon contacts were deposited on top. To achieve the NiO/ZnO layer stacking, the platen (printing stage) temperature was set to 35 °C during printing, inducing partial evaporation of the inks (based on low-boiling point solvents) between each layer.

**Instruments for Characterization:** The morphology of the inkjet-printed ZnO and NiO layers was studied by FE-SEM using a JEOL J-7100. The crystalline microstructure of the metal oxide nanoparticles was studied by XRD using a Japan Rigaku D/Max-IIA X-ray diffractometer using Cu K<sub>α</sub> radiation, λ = 1.5406 Å. UV-vis optical spectra in the range from 300 to 1100 nm were acquired from metal oxide layers printed on fused silica at room temperature. For this purpose, a Bentham PV300 EQE system was used where the monochromated light from a Xe lamp passes through the sample and the transmitted/reflected light was collected with an InGaAs photodetector placed within an integrating sphere. Finally, I-V

measurements were performed using an Agilent B1500 semiconductor device analyzer.

## Acknowledgements

The authors wish to thank the financial support from the European Commission via FET Open Grant (862656 – DROP-IT), MINECO (Spain) for grant PID2019-105658RB-I00 (PRITES project), Ministry of Science and Innovation of Spain under Project STABLE (PID2019-107314RB-I00), and Generalitat Valenciana via Prometeo Grant Q-Devices (Prometeo/2018/098).

## Conflict of Interest

The authors declare no conflict of interest.

## Data Availability Statement

The data that support the findings of this study are available from the corresponding author upon reasonable request.

## Keywords

diode, heterojunction, inkjet printing, metal oxides, nanoparticles, NiO, photodetector, ZnO

Received: January 12, 2023

Revised: February 28, 2023

Published online:

- [1] K. Nomura, A. Takagi, T. Kamiya, H. Ohta, M. Hirano, H. Hosono, *Jpn. J. Appl. Phys.* **2006**, *45*, 4303.
- [2] X. Yu, T. J. Marks, A. Facchetti, *Nat. Mater.* **2016**, *15*, 383.
- [3] J. A. Christians, R. C. M. Fung, P. v. Kamat, *J. Am. Chem. Soc.* **2014**, *136*, 758.
- [4] J. Meyer, S. Hamwi, M. Kröger, W. Kowalsky, T. Riedl, A. Kahn, *Adv. Mater.* **2012**, *24*, 5408.
- [5] K. Nomura, H. Ohta, A. Takagi, T. Kamiya, M. Hirano, H. Hosono, *Nature* **2004**, *432*, 488.
- [6] M. A. Haque, A. D. Sheikh, X. Guan, T. Wu, *Adv. Energy Mater.* **2017**, *7*, 1602803.
- [7] R. Jose, V. Thavasi, S. Ramakrishna, *J. Am. Ceram. Soc.* **2009**, *92*, 289.
- [8] I. Concina, A. Vomiero, *Small* **2015**, *11*, 1744.

- [9] T. Kamiya, H. Hosono, *NPG Asia Mater* **2010**, *2*, 15.
- [10] C. W. Litton, D. C. Reynolds, T. C. Collins, *Zinc Oxide Materials for Electronic and Optoelectronic Device Applications*, John Wiley & Sons, Chichester, UK, **2011**.
- [11] J. S. Park, W.-J. Maeng, H.-S. Kim, J.-S. Park, *Thin Solid Films* **2012**, *520*, 1679.
- [12] C. Dreyer, F. Mildner, *III-Nitride Ultraviolet Emitters*, Springer, Cham **2016**.
- [13] D. J. Gaspar, E. Polikarpov, *OLED Fundamentals*, CRC Press, Boca Raton, FL **2015**.
- [14] L. Nayak, S. Mohanty, S. K. Nayak, A. Ramadoss, *J Mater Chem C Mater* **2019**, *7*, 8771.
- [15] N. C. Raut, K. Al-Shamery, *J Mater Chem C Mater* **2018**, *6*, 1618.
- [16] W. Zapka, *Handbook of Industrial Inkjet Printing*, Wiley-VCH, Weinheim, Germany, **2017**.
- [17] M. Singh, H. M. Haverinen, P. Dhagat, G. E. Jabbour, *Adv. Mater.* **2010**, *22*, 673.
- [18] M. Gao, L. Li, Y. Song, *J. Mater. Chem. C* **2017**, *5*, 2971.
- [19] J. Arrese, G. Vescio, E. Xuriguera, B. Medina-Rodriguez, A. Cornet, A. Cirera, *J. Appl. Phys.* **2017**, *121*, 104904.
- [20] G. Vescio, J. López-Vidrier, R. Leghrib, A. Cornet, A. Cirera, *J Mater Chem C Mater* **2016**, *4*, 1804.
- [21] G. Vescio, J. L. Friero, A. F. Gualdrón-Reyes, S. Hernández, I. Mora-Seró, B. Garrido, A. Cirera, *Adv. Mater. Technol.* **2022**, *7*, 2101525.
- [22] G. Vescio, G. Martín, A. Crespo-Yepes, S. Claramunt, D. Alonso, J. López-Vidrier, S. Estradé, M. Porti, R. Rodríguez, F. Peiró, A. Cornet, A. Cirera, M. Nafria, *ACS Appl Mater Interfaces* **2019**, *11*, 23659.
- [23] G. Vescio, A. Crepo-Yepes, D. Alonso, S. Claramunt, M. Porti, R. Rodriguez, A. Cornet Calveras, A. Cirera Hernandez, M. Nafria, X. Aymerich, *IEEE Electron Device Lett.* **2017**, *38*, 457.
- [24] G. Vescio, J. Sanchez-Diaz, J. L. Friero, R. S. Sánchez, S. Hernández, A. Cirera, I. Mora-Seró, B. Garrido, *ACS Energy Lett.* **2022**, *7*, 3653.
- [25] S. Chung, K. Cho, T. Lee, *Adv. Sci.* **2019**, *6*, 1801445.
- [26] A. Heinrichsdobler, J. C. Roigk, F. Schirmeier, C. J. Brabec, T. Wehlius, *Adv. Mater. Technol.* **2017**, *2*, 1700166.
- [27] Ü. Özgür, D. Hofstetter, H. Morkoç, *Proc IEEE Inst Electr Electron Eng* **2010**, *98*, 1255.
- [28] Ü. Özgür, Y. I. Alivov, C. Liu, A. Teke, M. A. Reshchikov, S. Doğan, V. Avrutin, S.-J. Cho, H. Morkoç, *J. Appl. Phys.* **2005**, *98*, 041301.
- [29] R. F. Service, *Science* **1997**, *276*, 895.
- [30] Y. F. Li, B. Yao, R. Deng, B. H. Li, J. Y. Zhang, Y. M. Zhao, D. Y. Jiang, Z. Z. Zhang, C. X. Shan, D. Z. Shen, X. W. Fan, Y. M. Lu, *J Phys D Appl Phys* **2009**, *42*, 105102.
- [31] D. C. Look, *Mater. Sci. Eng., B* **2001**, *80*, 383.
- [32] A. Tsukazaki, A. Ohtomo, T. Onuma, M. Ohtani, T. Makino, M. Sumiya, K. Ohtani, S. F. Chichibu, S. Fuke, Y. Segawa, H. Ohno, H. Koinuma, M. Kawasaki, *Nat. Mater.* **2005**, *4*, 42.
- [33] Y.-H. Kim, J.-S. Heo, T.-H. Kim, S. Park, M.-H. Yoon, J. Kim, M. S. Oh, G.-R. Yi, Y.-Y. Noh, S. K. Park, *Nature* **2012**, *489*, 128.
- [34] M. S. Chavali, M. P. Nikolova, *SN Appl Sci* **2019**, *1*, 607.
- [35] M. D. Irwin, D. B. Buchholz, A. W. Hains, R. P. H. Chang, T. J. Marks, *Proc. Natl. Acad. Sci. USA* **2008**, *105*, 2783.
- [36] M. D. Irwin, J. D. Servaites, D. B. Buchholz, B. J. Leever, J. Liu, J. D. Emery, M. Zhang, J.-H. Song, M. F. Durstock, A. J. Freeman, M. J. Bedzyk, M. C. Hersam, R. P. H. Chang, M. A. Ratner, T. J. Marks, *Chem. Mater.* **2011**, *23*, 2218.
- [37] H. T. Nguyen, H. Jeong, J.-Y. Park, Y. H. Ahn, S. Lee, *ACS Appl. Mater. Interfaces* **2014**, *6*, 7286.
- [38] Y. Zhao, H. Wang, C. Wu, W. Li, F. Gao, G. Wu, B. Zhang, G. Du, *Opt. Commun.* **2015**, *336*, 1.
- [39] P. Zhai, Q. Yi, J. Jian, H. Wang, P. Song, C. Dong, X. Lu, Y. Sun, J. Zhao, X. Dai, Y. Lou, H. Yang, G. Zou, *Chem. Commun.* **2014**, *50*, 1854.
- [40] A. A. Ahmed, M. Devarajan, N. Afzal, *Sens Actuators A Phys* **2017**, *262*, 78.
- [41] R. Chen, L. Lan, *Nanotechnology* **2019**, *30*, 312001.
- [42] J. You, L. Meng, T.-B. Song, T.-F. Guo, Y. (Michael) Yang, W.-H. Chang, Z. Hong, H. Chen, H. Zhou, Q. Chen, Y. Liu, N. de Marco, Y. Yang, *Nat. Nanotechnol.* **2016**, *11*, 75.
- [43] S. Liu, R. Liu, Y. Chen, S. Ho, J. H. Kim, F. So, *Chem. Mater.* **2014**, *26*, 4528.
- [44] T. F. Chen, A. J. Wang, B. Y. Shang, Z. L. Wu, Y. L. Li, Y. S. Wang, *J. Alloys Compd.* **2015**, *643*, 167.
- [45] T. Zhang, L. Li, J.-P. Ao, *Surf. Interfaces* **2016**, *5*, 15.
- [46] A. O. M. Alzahrani, M. S. Abdel-wahab, M. Alayash, M. S. Aida, *Braz. J. Phys.* **2021**, *51*, 1159.
- [47] Y. H. Hwang, J. S. Seo, J. M. Yun, H. J. Park, S. Yang, S. H. K. Park, B. S. Bae, *NPG Asia Mater* **2013**, *5*, e45.
- [48] J. Socratous, K. K. Banger, Y. Vaynzof, A. Sadhanala, A. D. Brown, A. Sepe, U. Steiner, H. Sirringhaus, *Adv. Funct. Mater.* **2015**, *25*, 1873.
- [49] P. Calvert, *Chem. Mater* **2001**, *13*, 3299.
- [50] C. Belver, J. Bedia, J. J. Rodriguez, A. Gómez-Avilés, M. Peñas-Garzón, in *Nanoscale Materials in Water Purification*, Elsevier, Amsterdam **2019**.
- [51] A. Barhoum, H. Rahier, M. Benelmekki, G. van Assche, in *Fundamentals of Nanoparticles: Classifications, Synthesis Methods, Properties and Characterization*, Elsevier, Amsterdam **2018**.
- [52] I. Udom, M. K. Ram, E. K. Stefanakos, A. F. Hepp, D. Y. Goswami, *Mater. Sci. Semicond. Process.* **2013**, *16*, 2070.
- [53] H. Swanson, E. Tatge, *Standard X-Ray Diffraction Powder Patterns*, National Bureau of Standards, Gaithersburg, MD **1966**.
- [54] J. D. Hanawalt, H. W. Rinn, L. K. Frevel, *Ind. Eng. Chem., Anal. Ed.* **1938**, *10*, 457.
- [55] D. Soltman, V. Subramanian, *Langmuir* **2008**, *24*, 2224.
- [56] W. M. Haynes, *CRC Handbook of Chemistry and Physics*, CRC Press, Boca Raton, FL **2011**.
- [57] S. A. Mahmoud, A. Shereen, M. A. Tarawnh, *J. Mod. Phys.* **2011**, *02*, 1178.
- [58] S. Liu, R. Liu, Y. Chen, S. Ho, J. H. Kim, F. So, *Chem. Mater.* **2014**, *26*, 4528.
- [59] P. Zhai, Q. Yi, J. Jian, H. Wang, P. Song, C. Dong, X. Lu, Y. Sun, J. Zhao, X. Dai, Y. Lou, H. Yang, G. Zou, *Chem. Commun.* **2014**, *50*, 1854.
- [60] K. N. Manjunatha, S. Paul, *Appl. Surf. Sci.* **2015**, *352*, 10.
- [61] W. Xu, J. Zhang, Y. Li, L. Zhang, L. Chen, D. Zhu, P. Cao, W. Liu, S. Han, X. Liu, Y. Lu, *J. Alloys Compd.* **2019**, *806*, 40.
- [62] G. Dasi, R. Ramarajan, D. P. Joseph, S. Vijayakumar, J. J. Shim, M. Arivananthan, R. Jayavel, K. Thangaraju, *Thin Solid Films* **2020**, *710*, 138265.
- [63] J. H. Lee, K. H. Ko, B. O. Park, *J. Cryst. Growth* **2003**, *247*, 119.
- [64] S. Bose, C. Chevallier, S. O. Saad Hamady, D. Horwat, J. F. Pierson, P. Boulet, T. Gries, T. Aubert, N. Fressengeas, *Superlattices Microstruct.* **2021**, *156*, 106945.
- [65] C. Y. Tsay, K. S. Fan, S. H. Chen, C. H. Tsai, *J. Alloys Compd.* **2010**, *495*, 126.
- [66] S. Y. Tsai, M. H. Hon, Y. M. Lu, *Solid State Electron* **2011**, *63*, 37.
- [67] D. Y. Kim, J. Ryu, J. Manders, J. Lee, F. So, *ACS Appl. Mater. Interfaces* **2014**, *6*, 1370.
- [68] N. Park, K. Sun, Z. Sun, Y. Jing, D. Wang, *J. Mater. Chem. C* **2013**, *1*, 7333.
- [69] J. Huang, B. Li, Y. Hu, X. Zhou, Z. Zhang, Y. Ma, K. Tang, L. Wang, Y. Lu, *Surf. Coat. Technol.* **2019**, *362*, 57.
- [70] K. Wang, Y. Vygranenko, A. Nathan, *Thin Solid Films* **2008**, *516*, 1640.
- [71] H. Ohta, M. Hirano, K. Nakahara, H. Maruta, T. Tanabe, M. Kamiya, T. Kamiya, H. Hosono, *Appl. Phys. Lett.* **2003**, *83*, 1029.
- [72] J. Leppaniemi, K. Eiroma, H. S. Majumdar, A. Alastalo, *IEEE Electron Device Lett.* **2016**, *37*, 445.